Published in final edited form as:
J Pathol. 2015 January ; 235(1): 25–36. doi:10.1002/path.4443.

MiR-506 inhibits multiple targets in the epithelial-to-mesenchymal transition network and is associated with good prognosis in epithelial ovarian cancer

Yan Sun[1,3], **Limei Hu**[3], **Hong Zheng**[2], **Marina Bagnoli**[6], **Yuhong Guo**[1], **Rajesha Rupaimoole**[4,5], **Cristian Rodriguez-Aguayo**[4,5], **Gabriel Lopez-Berestein**[4,5], **Ping Ji**[3], **Kexin Chen**[2], **Anil K. Sood**[4,5], **Delia Mezzanzanica**[6], **Jinsong Liu**[3], **Baocun Sun**[1], and **Wei Zhang**[3,5,*]

[1]Department of Pathology, Tianjin Medical University Cancer Institute and Hospital, Tianjin 300060, China

[2]Department of Epidemiology and Biostatistics, Tianjin Medical University Cancer Institute and Hospital, Tianjin 300060, China

[3]Department of Pathology, The University of Texas MD Anderson Cancer Center, Houston, TX 77030, USA

[4]Department of Gynecologic Oncology and Reproductive Medicine, The University of Texas MD Anderson Cancer Center, Houston, TX 77030, USA

[5]Center for RNAi and Non-Coding RNA, The University of Texas MD Anderson Cancer Center, Houston, TX 77030, USA

[6]Department of Experimental Oncology and Molecular Medicine, Fondazione IRCCS Istituto Nazionale dei Tumori, Milan, Italy

Abstract

Extensive investigations have shown that miRNAs are important regulators of epithelial-to-mesenchymal transition (EMT), mainly targeting the transcriptional repressors of E-cadherin (Ecad). Less is known about the post-transcriptional regulation of vimentin or N-cadherin (N-cad) in EMT. Our previous study identified miR-506 as a key EMT inhibitor through directly targeting the E-cad transcriptional repressor, SNAI2. In this study, we provide evidence that miR-506 simultaneously suppresses vimentin and N-cad. The knockdown of vimentin using siRNA reversed EMT, suppressed cell migration and invasion, and increased E-cad expression on cell membrane in epithelial ovarian cancer (EOC) cells. In a set of tissue microarrays that included 204 EOCs of all major subtypes (e.g., serous, endometrioid, clear cell, and mucinous), miR-506 was positively correlated with E-cad and negatively correlated with vimentin and N-cad in all subtypes

*Address correspondence to Wei Zhang, Department of Pathology, Unit 85, The University of Texas MD Anderson Cancer Center, 1515 Holcombe Blvd., Houston, TX 77030, USA; tel: 713 745 1103; fax: 713 792 5549; wzhang@mdanderson.org.

The authors declare that no conflict of interest exists.

Author contributions

Y. S., H. L., H. Z., M. B., Y. G., R. R., C. R., G. L., and P. J. performed experiments; Y. S., K. C., A. K. S., D. M., J. L, B. S. and W.Z. designed the studies. Y. S., H. L., P. J. A. K. S., D. M., J. L, B. S., and W.Z. wrote the manuscript. All authors read and approved the final manuscript.

of EOC. A high level of miR-506 was positively associated with early FIGO stage and longer survival in EOC. Introduction of miR-506, mediated by nanoparticle delivery, in EOC orthotopic mouse models resulted in decreased vimentin, N-cad, and SNAI2 expression and increased E-cad expression; it also suppressed the dissemination of EOC cells. Thus, miR-506 represents a new class of miRNA that regulates both E-cad and vimentin/N-cad in the suppression of EMT and metastasis.

Keywords

miR-506; epithelial-to-mesenchymal transition; vimentin; N-cadherin; epithelial ovarian cancer; nanoparticle

Introduction

Epithelial ovarian cancer (EOC) remains the most lethal gynecological malignancy [1]. The majority of EOC patients are diagnosed at advanced stages and the overall 5-year survival rate is around 40% [2]. Although EOC is a heterogeneous disease, the standard treatment for EOC patients remains a combination of cytoreductive surgery and platinum-based chemotherapy [2]. Many targeted therapies, including anti-angiogenic agents and PARP inhibitors, are currently under evaluation in phase I/II and III studies [3–6].

Epithelial-to-mesenchymal transition (EMT) is a well-recognized dedifferentiation process that is critical for epithelial cancer metastasis [7]. Therefore, EOC patients may benefit from targeted therapies that inhibit EMT. The process of EMT is highly coordinated and involves complex gene expression reprograming [8,9]. The molecular hallmarks of EMT include down-regulation of E-cadherin (E-cad), which is responsible for cell-cell adhesion, and up-regulation of mesenchymal proteins, such as vimentin and N-cadherin (N-cad). E-cad has been the focus of EMT regulation and is considered a driver for this process [8,10–13]. In contrast, vimentin and N-cad, although they are evaluated in almost all EMT studies, have been considered as markers with functional role not well understood.

In addition to transcription factors, EMT is regulated by post-transcriptional mechanisms, including microRNAs (miRNAs) [8,9,14]. MiRNAs are a class of small non-coding RNAs (~22 nt) that regulate 30% of the transcriptome by binding to the 3′-untranslated region (3′-UTR) of target genes, leading to either mRNA degradation or inhibition of protein translation [15]. Increasing evidence has demonstrated that miRNAs are highly deregulated in cancer, suggesting that they function as therapeutic targets [16,17]. Extensive investigations have shown that miRNAs are important regulators of EMT and mainly target E-cad transcription repressors, such as the let-7 and miR-200 miRNA families [18,19]. Recently, miR-30a and miR-138 were shown to directly target VIM [20,21]. Few miRNAs have been reported to regulate both E-cad and esenchymal proteins.

Our recent investigation of the EMT regulatory network in the serous subtype of EOC characterized miR-506 as a robust EMT inhibitor through directly targeting E-cad repressor SNAI2 [14]. In further computational analyses, we found a single miR-506 binding site in the 3′-UTRs of both the vimentin gene (*VIM*) and N-cad gene (*CDH2*), suggesting that

miR-506 is a member of a new class of EMT regulatory miRNAs that affect multiple targets in EMT processes. Here we provide experimental evidence that miR-506 directly targets vimentin and N-cad.

Materials and Methods

MiRNA transfection, and siRNA transfection

The miRNA mimics of miR-506 and negative controls were obtained from Dharmacon (Chicago, IL, USA). Cells were seeded at 2×10^5 per well in 6-well plates and allowed to attach for at least 16 hours. MiR-506 mimic or negative control was transfected using lipofectamine RNAiMAX (Invitrogen) at a final concentration of 50 nM.

SiRNAs against vimentin (ID# s14799 and s14800) were purchased from Ambion by Life Technologies. The si-RNA transfection was performed the same way as that for miRNAs, as described above. The final siRNA concentration was 50 nM. For the sustained si-RNA knock down experiments, the cells were transfected with the siRNA 3 times in a 4-day interval. The cells were split at a 1:2 ratio at 3 days post-transfection.

Western blot analysis

Primary antibodies of β-actin and vimentin were obtained from Santa Cruz Biotechnology (Santa Cruz, CA, USA), Sigma (Woodlands, TX, USA), or Novocastra (Newcastle Upon Tyne, UK). N-cadherin antibodies were purchased from Cell Signaling Technology (Boston, MA, USA) or BD Trasduction Laboratories (San Jose, CA, USA). A Western blot analysis was performed as described previously [14]. The detailed method can be found in online Supporting Information.

Immunofluorescence staining and confocal imaging

Cells were seeded into 15 μ-Slide VI purchased from ibidi (# 80602) and cultured in complete medium. Cells were fixed in 4% paraformaldehyde for 15 min, followed by permeabilization in 1x PBS containing 0.5% NP40 for 30 min at ambient temperature. The cells were blocked in blocking solution (1x PBS containing 10% normal goat serum and 0.5% NP40) for at least 4 hours and incubated with a mouse monoclonal anti-human E-cad or vimentin antibody (1:200 dilution) at 4°C overnight. After being washed, the cells were incubated with a goat anti-mouse IgG conjugated with Alexa Fluor 488 (Invitrogen, #A11029) (1:1000 dilution) at ambient temperature for 1 hour. F-actin was stained with phalloidin-TRITC (Molecular Probes, Invitrogen) at a concentration of 0.5 μg/mL and incubated at ambient temperature for 45 min. The images were taken by an Olympus FV1000 laser confocal microscope. Phase images were captured using a Zeiss HAL 100 microscope.

MiR-506 binding site deletion and luciferase reporter assay

The 3′-UTR of *VIM* that contains the predicted binding site of miR-506 was amplified from normal fetal genomic DNA by PCR using specific primers (online Supporting Information). The PCR product was cloned into the pGL3-control vector at the Xba I site in the correct direction. The consensus miR-506 binding site was deleted by PCR using a QuikChange II

XL site-directed mutagenesis kit (Stratagen). All clones were verified by DNA sequencing. For the luciferase reporter assay, subconfluent SKOV3 cells in 12-well plates were transfected with a triplicate repeat of pGL3 reporter plasmid (0.5 μg), pRL-TK (20 ng), miRmimics or negative controls (50 nM), and lipofectamine 2000 (2 μL) (Invitrogen). Twenty-four hours after transfection, cells were lysed and luciferase activities were determined as for a dual-luciferase assay reporter system (Promega), according to the manufacturer's instructions.

A 25 bp region of the 3′UTR *CDH2* gene containing the miR-506 seed region was cloned in the pmiR-Glo Dual Luciferase miRNA Target Expression Vector (Promega) according to the manufacturer's instructions. The specific primer sequences can be found in online Supporting Information. All clones were verified by DNA sequencing. For the luciferase assay, 5×10^4 HEK293T and OAW42 cells were seeded in triplicate in 24-well plates and transfected 24 h with pmiRGlovector (1 μg) together with 50 nM miR-506 mimics, unrelated miR, or scrambled miR as a negative control.

Cell migration and invasion assays

Wound healing and Transwell invasion assays were performed as described previously [14]. In brief, 70 μl of cells (5×10^5/ml) were seeded into a μ-Dish 35-mm high Culture-Insert (ibidi) and cultured for 24 hours. Then the wound was applied, and phase-microscopy imaging was performed at different time periods. The cell invasion assay was performed in duplicate using Matrigel-coated transwell chambers (8-μm pore size, BD). The cells were plated in 500 μl of serum-free medium (4×10^4 cells per transwell) and allowed to invade towards a 10% FBS medium for 20 h. Cells that invaded into the underside of the filter were fixed and stained with HEMA-DIFF solution (Fisher). The numbers of invaded cells from 5 randomly chosen fields were counted for each membrane.

Patient tissue samples and tissue microarray construction

We collected paraffin-embedded tissue from 204 EOC cases from Tianjin Medical University Cancer Institute and Hospital after we received approval from the institutional review board. The clinical characteristics of the cases are listed in Table 1. These samples were collected for tissue microarray (TMA) analyses. TMAs were constructed using a manual tissue microarray instrument (Beecher Instruments) equipped with a 2.0-mm punch needle, as described in a previous study [14].

MiRNA *in situ* hybridization

MiRNA *in situ* hybridization (ISH) was performed as described previously [14]. The TMA slides were hybridized with the double-DIG-labeled miRCURY LNA™ detection probe, hsa-miR-506 (38314–15, Exiqon), for 2 hours at 55°C (Ventana Discovery Ultra). The digoxigenins were detected with a polyclonal anti-DIG antibody and an alkaline phosphatase-conjugated second antibody (Ventana), using NBT-BCIP as the substrate. The LNA U6 snRNA probe was used as a positive control for every TMA core. Signals in tumor cells were quantified as described previously [14], using a scoring system from 0 to 9, multiplied signal intensity and the percentage of positive cells (signal: 0 = no signal, 1 = weak signal, 2 = intermediate signal, and 3 = strong signal; percentage: 0 = 0%, 1 = <25%, 2

= 25%–50%, and 3 = >50%). Low and high MiR-506 expression levels were defined as scores of <6 and ≥6, respectively.

Immunohistochemical analysis

Immunohistochemical staining was performed with the mouse anti-human N-cadherin (1:100, 3B9, Invitrogen), mouse anti-human vimentin (1:50, V9, Santa Cruz), rabbit anti-human SNAI2 (1:10, C19G7, Cell Signaling Technology), and rabbit anti-human E-cadherin (1:100, H-108, Santa Cruz) antibodies on TMA sections after antigen retrieval. Dako EnVision+ System-HRP (DAB) kits were used. For the negative controls, the primary antibodies were replaced with PBS. N-cadherin- and vimentin-positive cells were defined as those with brown staining in the cytoplasm, whereas SNAI2- and E-cadherin-positive cells were defined as those with brown staining in the nucleus and cell membrane, respectively. Signals in tumor cells were quantified using the same scoring system (0–9) as that for miRNA ISH, described above.

Liposomal preparation

MiRNA for *in vivo* delivery was incorporated into DOPC (1,2-dioleoyl-*sn*-glycero-3-phosphatidylcholine) as previously described [14]. DOPC and miRNA were mixed in the presence of excess tertiary butanol at a ratio of 1:10 (w/w) miRNA/DOPC. Tween 20 was added to the mixture of Tween 20 and miRNA/DOPC in a ratio of 1:19. The mixture was vortexed, frozen in an acetone/dry ice bath, and lyophilized. Before *in vivo* administration, the preparation was hydrated with PBS at ambient temperature at a concentration of 200 μg/kg per injection.

Animals, orthotopic models, and tissue processing

Forty female athymic nude mice were purchased from the National Cancer Institute, Frederick Cancer Research and Development Center (Frederick, MD). They were cared for according to guidelines set forth by the American Association for Accreditation of Laboratory Animal Care and the U.S. Public Health Service Humane Care and Use of Laboratory Animals policy. All mouse studies were approved and supervised by the MD Anderson Institutional Animal Care and Use Committee. All animals were 8–12 weeks of age at the time of injection. HeyA8-IP2 and SKOV3-IP1 cells were trypsinized, washed, resuspended in Hank's balanced salt solution (Gibco, Carlsbad, CA), and injected into the peritoneal cavities of mice (1.0×10^6 cells/mouse). Seven days after tumor cell injection, mice were randomly separated into 2 groups (n = 10 mice per group) and treated with miRNA incorporated in DOPC nanoliposomes (intraperitoneal administration): control miRNA/DOPC or miR-506/DOPC. Twice-weekly treatments continued for 4–6 weeks, at which point, all mice were killed and necropsied, and their tumors were harvested.

Tumor tissue was snap frozen or fixed in formalin. Hematoxylin and eosin (H&E) and immunohistochemical staining was performed. For immunohistochemical staining, rabbit anti-human polyclonal antibody against N-cad (1:250, Boster Biological Technology, Wuhan, China) and Dako EnVision+ System-HRP Rabbit (DAB) were used. The calculation method for N-cad was the same as that for TMA, as described above.

Statistical analysis

Student's t test, chi-square test, Fisher's exact test, Kaplan-Meier analyses, and log-rank tests were performed using SPSS software version 17.0. Significance was defined as $P < 0.05$.

Results

MiR-506 directly targets *VIM* and *CDH2* expression through 3′-untranslated regions

An examination of 7 publicly available miRNA target gene databases revealed that *VIM* and *CDH2* had 1 predicted binding site of miR-506 (Figure 1A). Transfection of miR-506 mimic in 3 EOC cell lines led to decreased VIM and N-cad protein levels (Figure 1B). To determine whether miR-506 regulates *VIM* through binding to its 3′-UTR, we cloned the *VIM* 3′-UTR into the pmirGLO luciferase reporter vector and transfected the pmirGLO vector or the parent luciferase expression vector, with miR-506 mimic or miR-ctrl, into SKOV3 cells. Co-transfection of pmirGLO-*VIM*-3′-UTR and miR-506 mimic resulted in lower luciferase activity than that in the cells co-transfected with miR-ctrl (P=0.009, Figure 1C), suggesting that miR-506 directly targets *VIM*. To confirm that miR-506 specifically regulates *VIM*, we generated the construct pmirGLO-VIM-3′-UTR-mutant in which the miR-506 binding site sequence on the 3′-UTR was deleted. These constructs were then co-transfected with miR-506 mimic or miR-ctrl into SKOV3 cells. Deletion of the miR-506 binding site from the 3′-UTRs abolished the effects of miR-506 on luciferase activity (Figure 1C). For *CDH2* targeting, we cloned a small region of 25 bp that contained the miR-506 seed into the pmRGLO vector to avoid interference with other miRNAs that may target the 3′UTR of *CDH2*. HEK293T cells and the OAW42 EOC cell line were then transfected with reporter plasmid alone or in association with a scrambled miR, miR506 mimic, or unrelated miR. A significant decrease in luciferase activity was observed in miR-506-transfected cells, demonstrating direct binding of the selected miRNA within the predicted 3′UTR of *CDH2* (Figure 1D).

Attenuation of vimentin induces epithelial characteristics and suppresses cell migration and invasion

Vimentin is an intermediate cell filament protein that is commonly considered as a mesenchymal marker. Vimentin's functional role in the EMT process is not well understood. To gain insight into the vimentin's function, we treated OVCA433 OvCa cells with siRNAs against vimentin. As shown in Figure 2A, at 72 h after transfection, both siRNAs led to a significant decrease of vimentin compared with that in the si-control transfected cells (Figure 2A). Interestingly, E-cadherin levels in the transfected cells were increased (Figure 2A). An immunofluorescence staining analysis showed that the cells with significantly low levels of vimentin exhibited epithelial cell morphological characteristics, characterized by plump and aggregated cells and a cortical f-actin staining pattern (Figure 2B, upper panel, arrows). On the other hand, a fraction of cells with relatively high levels of vimentin still showed the mesenchymal phonotype, characterized by spreading growth and the mesenchymal f-actin staining pattern (Figure 2B, upper panel, arrow heads). The cells transfected with si-VIM exhibited intense E-cad expression on cell membranes in cell-cell

junctions (Figure 2B, lower panel). In the wound healing assay, we observed moderate inhibition of cell migration at 72 h after si-VIM treatment (Figure 2C).

We next performed a sustained knockdown of vimentin by continually transfecting the siRNAs to the OVCA433 cells for 12 days (3 times in a 4-day interval). The majority of si-VIM transfected cells showed undetectable levels of vimentin (Fig 2D, upper panel) and marked epithelial honeycomb morphological characteristics, characterized by the co-localization of Ecad and f-actin in the cell-cell junctions (Fig. 2D, lower panel). Consistently, we observed a significant inhibition of cell migration and invasion after the sustained knock-down of vimentin (Figure 2E, F). Similar results were observed in SKOV3 cells (Figure 2G, H). In contrast to the results of siRNA experiments for vimentin, we did not observe marked changes in cell migration and invasion when we treated SKOV3 cells with siRNA for N-cad.

MiRNA-506 expression is associated with decreased vimentin, N-cad, and SNAI2 expression and increased E-cad expression in all major subtypes of EOC

In our previous study, we reported that miR-506 levels, as quantified by real-time PCR, were consistent with miR-506 ISH results, and associated with decreased SNAI2 and vimentin and increased E-cad expression in high-grade serous OvCa [14]. In this study, with a comprehensive TMA, we quantified the expression of miR-506, control U6 small RNA, vimentin, N-cad, SNAI2, and E-cad in the tumor cells of 204 EOCs including the 92 serous OvCa cases that were used in our previous study [14]. Although snail transcriptional factors (SNAI1/2) have been detected in both cytoplasm and nucleus [22–24], we focused our quantification of nuclear SNAI2 pertaining to its function as a nuclear transcriptional suppression of E-cad. MiR-506 expression can be evaluated in 99 serous, 74 endometrioid, 9 mucinous, 8 clear cell, 4 mixed, and 2 undifferentiated OvCa cases. In serous OvCa, miR-506 expression was negatively correlated with SNAI2 and vimentin and positively correlated with E-cad (Figure 3A, Table 2), which was consistent with the findings of our previous report [14]. Furthermore, the negative correlation was found between miR-506 and N-cad expression in serous OvCa (Figure 3A, Table 2). The same correlations of miR-506 expression with EMT proteins were found in endometrioid OvCa (Figure 3B, Table 2). Although our study included a limited number of cases, similar correlations or trends were observed in mucinous and clear cell OvCa (Figure 3C, D, Table 2). Altogether, miR-506 expression was associated with decreased vimentin, N-cad, and SNAI2 expression and increased E-cad expression in the whole cohort of EOC cases (Table 2).

High miRNA-506 expression is associated with early FIGO stage and longer survival in EOC patients

With the expanded cohort of all the major subtypes of EOC, we analyzed the relationships between miR-506 and clinicopathologic parameters in EOC patients. The levels of miR-506 expression were comparable among different EOC subtypes or grades ($P>0.05$, Supplementary Table 1). High levels of miR-506 expression were associated with early FIGO stage in serous ($P=0.013$, Figure 4A) and endometrioid OvCa ($P=0.036$, Figure 4B), as well as all EOC cases ($P=0.001$, Figure 4C, Supplementary Table 1). Our previous study demonstrated that high miR-506 level, as estimated by qRT-PCR, was associated with

longer survival in high-grade serous OvCa [14]. Here, our results showed that higher miR-506 expression was significantly correlated with longer overall survival (OS) and progression-free survival (PFS) in all EOC patients (P=0.001, Figure 4D; P=0.001, Figure 4G). Because miR-506 expression was correlated with stage (Figure 4C, Supplementary Table 1) and stage was correlated with survival status and PFS (Supplementary Table 2), we further analyzed OS and PFS in both stage II and advanced stage and showed that the patients with high miR-506 expression exhibited a trend of longer OS than those with low miR-506 expression in both stages (P =0.070, Figure 4E; P=0.051, Figure 4F). Further, the patients with high miR-506 expression had longer PFS than those with low miR-506 expression in both stage II and advanced-stages (P=0.033, Figure 4H; P=0.047, Figure 4I). These results suggested that miR-506 downregulation accompanies the progression of EOC and miR-506 can be used as a prognostic predictor for EOC patients.

Systemic delivery of miR-506 suppresses invasion and metastasis of EOC cells in mouse models

To determine the effect of miR-506 on EOC progression, we established EOC orthotopic mouse models by intraperitoneally injecting mice with 2 EOC cell lines (SKOV3-IP1 and HeyA8-IP2) and treating them with miR-506-DOPC or miR-Ctrl-DOPC. Compared with miR-Ctrl-DOPC treatment, miR-506-DOPC treatment led to decreased VIM and SNAI2 and increased E-cad expression, as well as significant tumor suppression in both mouse models [14]. In this study, we examined the N-cad expression in tumors using immunohistochemical staining and verified that miR-506 also downregulated N-cad (Figure 5A, B). To further determine whether miR-506 can inhibit EOC dissemination in orthotopic mouse models, we carefully examined the organs in the pelvic and abdominal cavities. The mesentery, omentum, perihepatic, perisplenic, diaphragm, peritoneum, retroperitoneum, ovaries, and pelvis were involved by EOC cells (Supplementary Table 3, Figure 5C, D). Compared with the miR-Ctrl treatment groups, the miR-506 treatment groups had fewer invaded organs (P=0.152 for SKOV3, P=0.010 for HeyA8, Figure 5E). In addition, liver metastasis was only found in 2 mice that had been injected with HeyA8-IP2 cells and treated with miR-Ctrl (Figure 5F, G). No liver metastasis was found in either miR-506 treatment group. Together with the previous results [14], our orthotopic mouse models showed that miR-506 reduced the expression of VIM, N-cad, and SNAI2; increased the expression of E-cad; and eventually, inhibited EOC invasion and metastasis.

Discussion

EMT is regulated by complex networks that involve both transcriptional and post-transcriptional regulation [8,9,14]. In our previous study, we established that miR-506 is a key suppressor of EMT by directly targeting 3 binding sites on the 3′-UTR of SNAI2, a transcript suppressor of E-cad, thus increasing E-cad expression [14]. In the present study, we tested and validated a broader role for miR-506 in the suppression of EMT through the direct regulation of 2 recognized mesenchymal marker proteins, vimentin and N-cad. Therefore, miR-506 has emerged as a key network gatekeeper for epithelial and mesenchymal lineage switches by simultaneously regulating multiple nodes in the sophisticated regulatory network, as we have illustrated in a model (Figure 6). This model is

a simplified version that will likely be modified in future studies. For example, our recent study showed that miR-506 inhibited the expression of Forkhead box protein M1 (FoxM1) through directly downregulating CDK4/CDK6 [25]. FoxM1 was reported to be a transcriptional activator of SNAI1, another major E-cad repressor [26,27]. Therefore, miR-506 increases E-cad expression through multiple paths. In a recent publication, miR-506 was reported to target NFκB p65 [28], which was implicated in EMT regulation. Kuphal S *et al*. identified the NFκB-binding site in the N-cad promoter and reported that loss of E-cad could activate NFκB and induce N-cad expression during EMT of melanoma cells [29]. Vimentin expression was also reported to be transactivated by NFκB [30]. Although we consider E-cad and vimentin/N-cad to be the 2 spectrums of EMT/MET, key proteins in these 2 processes have close crosstalk, and there must be extensive feedback regulations between them. In the present study, we found that the knockdown of vimentin upregulated E-cad expression. It was reported by Rodriguez et al. that vimentin inhibited E-cad and induced EMT through GSK-3β, which is an upstream regulator of SNAI1 [31]. Therefore, miR-506 represents a gatekeeper class of EMT inhibitory microRNAs that target multiple key node genes that patrol the EMT network.

A second major finding of this study is that vimentin is not just an indicator or marker for EMT. We demonstrated that the knockdown of vimentin alone was sufficient to suppress EMT in EOC cells, including increasing E-cad expression and cell-cell adhesion, inducing actin cytoskeleton reorganization, causing more epithelial morphological characteristics, and inhibiting cell migration and invasion. Rodriguez et al. also found that vimentin expression was sufficient to induce increased mesenchymal and pro-metastatic phenotypical changes in melanoma cells, including ILK/GSK-3β-dependent E-cad down-regulation, Snail1 activation, and increased cell motility and migration [31]. Therefore, vimentin may be directly involved in the modulation of EMT and may play an important role in cancer progression. The results of our *in vitro* cell-based studies suggested a weaker role of N-cad in EMT and the cell migration and invasion process. It should be noted that N-cad is known to mediate the cell-stromal interaction [32]. The current experimental systems do not sufficiently consider the stromal component, which may explain the weaker effect observed in our experiments. Future experiments that include multiple cellular components (e.g., tumor cells and fibroblast co-cultures) should be able to better determine the role of N-cad.

Consistent with the *in vitro* results, miR-506 was associated with blocked EMT in all major subtypes of EOC in this study. Although EOC is considered as a heterogeneous disease, the majority of EOC patients were diagnosed at advanced stages with intraperitoneal dissemination and metastasis. Therefore, miR-506 may exert a multifaceted anti-metastatic effect to counteract the progression of all major subtypes of EOC. In addition, the role of miR-506 in EMT inhibition and in cell senescence and differentiation was recently demonstrated in several cancer types, including ovarian, breast, lung, and cervical cancer and neuroblastoma [14,25,28,33–35]. Our previous and present studies showed that miR-506, when delivered through a nanoparticle vehicle, effectively reduced the tumor burden and inhibited invasive growth and metastasis in EOC orthotopic mouse models. The nanoparticle-mediated delivery of tumor suppressive miRNAs has been actively explored as a new strategy for cancer therapeutics [16,36,37]. Therefore, miR-506 may represent a

promising new therapeutic agent that can be carried by this new tool to suppress EMT and cancer progression in a broad spectrum of cancer types.

Supplementary Material

Refer to Web version on PubMed Central for supplementary material.

Acknowledgments

We thank Ms. Ann Sutton in the Department of Scientific Publications for editing this manuscript and Jared Burks (Flow Cytometry & Cellular Imaging Core Facility) for technical assistance. This study was partially supported by U.S. National Institutes of Health grants U24CA143835, P50 CA083639, and U54 CA151668, MD Anderson Cancer Center support grant CA016672, a grant from the Blanton-Davis Ovarian Cancer Research Program, a grant from the Asian Foundation for Cancer Research to W.Z., grants from the Program for Changjiang Scholars and Innovative Research Team in University (PCSIRT) in China and the National Key Scientific and Technological Project (2011ZX0 9307-001-04) and Tianjin Science and Technology Committee Foundation (09ZCZDSF04700) to K.C., a grant from NSF in China (#81201651) to Y.S., and a grant from Fondazione CARIPLO (2013-0865) to D.M.. The Tianjin Cancer Hospital Tumor Tissue Facility is jointly funded by the National Foundation for Cancer Research. Y.S. was supported by The A. Lavoy Moore Endowment Fund.

References

1. Siegel R, Naishadham D, Jemal A. Cancer statistics, 2013. CA Cancer J Clin. Jan; 2013 63(1):11–30. [PubMed: 23335087]
2. Banerjee S, Kaye SB. New strategies in the treatment of ovarian cancer: current clinical perspectives and future potential. Clin Cancer Res. Mar 1; 2013 19(5):961–968. [PubMed: 23307860]
3. Burger RA, Brady MF, Bookman MA, et al. Incorporation of bevacizumab in the primary treatment of ovarian cancer. N Engl J Med. Dec 29; 2011 365(26):2473–2483. [PubMed: 22204724]
4. Perren TJ, Swart AM, Pfisterer J, et al. A phase 3 trial of bevacizumab in ovarian cancer. N Engl J Med. Dec 29; 2011 365(26):2484–2496. [PubMed: 22204725]
5. Gelmon KA, Tischkowitz M, Mackay H, et al. Olaparib in patients with recurrent high-grade serous or poorly differentiated ovarian carcinoma or triple-negative breast cancer: a phase 2, multicentre, open-label, non-randomised study. Lancet Oncol. Sep; 2011 12(9):852–861. [PubMed: 21862407]
6. Ledermann J, Harter P, Gourley C, et al. Olaparib maintenance therapy in platinum-sensitive relapsed ovarian cancer. N Engl J Med. Apr 12; 2012 366(15):1382–1392. [PubMed: 22452356]
7. Kalluri R. EMT: when epithelial cells decide to become mesenchymal-like cells. J Clin Invest. Jun; 2009 119(6):1417–1419. [PubMed: 19487817]
8. Thiery JP, Sleeman JP. Complex networks orchestrate epithelial-mesenchymal transitions. Nat Rev Mol Cell Biol. Feb; 2006 7(2):131–142. [PubMed: 16493418]
9. Kalluri R, Weinberg RA. The basics of epithelial-mesenchymal transition. J Clin Invest. Jun; 2009 119(6):1420–1428. [PubMed: 19487818]
10. Kurahara H, Takao S, Maemura K, et al. Epithelial-mesenchymal transition and mesenchymal-epithelial transition via regulation of ZEB-1 and ZEB-2 expression in pancreatic cancer. J Surg Oncol. Jun 1; 2012 105(7):655–661. [PubMed: 22213144]
11. Batlle E, Sancho E, Franci C, et al. The transcription factor snail is a repressor of E-cadherin gene expression in epithelial tumour cells. Nat Cell Biol. Feb; 2000 2(2):84–89. [PubMed: 10655587]
12. Yang J, Mani SA, Donaher JL, et al. Twist, a master regulator of morphogenesis, plays an essential role in tumor metastasis. Cell. Jun 25; 2004 117(7):927–939. [PubMed: 15210113]
13. Fang X, Cai Y, Liu J, et al. Twist2 contributes to breast cancer progression by promoting an epithelial-mesenchymal transition and cancer stem-like cell self-renewal. Oncogene. Nov 24; 2011 30(47):4707–4720. [PubMed: 21602879]
14. Yang D, Sun Y, Hu L, et al. Integrated analyses identify a master microRNA regulatory network for the mesenchymal subtype in serous ovarian cancer. Cancer Cell. Feb 11; 2013 23(2):186–199. [PubMed: 23410973]

15. Esquela-Kerscher A, Slack FJ. Oncomirs - microRNAs with a role in cancer. Nat Rev Cancer. Apr; 2006 6(4):259–269. [PubMed: 16557279]
16. Iorio MV, Croce CM. MicroRNA dysregulation in cancer: diagnostics, monitoring and therapeutics. A comprehensive review. EMBO Mol Med. Mar; 2012 4(3):143–159. [PubMed: 22351564]
17. Liu M, Zhang X, Hu CF, Xu Q, Zhu HX, Xu NZ. MicroRNA-mRNA functional pairs for cisplatin resistance in ovarian cancer cells. Chin J Cancer. Jun 5; 2014 33(6):285–294. [PubMed: 24589211]
18. Peter ME. Let-7 and miR-200 microRNAs: guardians against pluripotency and cancer progression. Cell Cycle. Mar 15; 2009 8(6):843–852. [PubMed: 19221491]
19. Ding XM. MicroRNAs: regulators of cancer metastasis and epithelial-mesenchymal transition (EMT). Chin J Cancer. Mar; 2014 33(3):140–147. [PubMed: 24016392]
20. Cheng CW, Wang HW, Chang CW, et al. MicroRNA-30a inhibits cell migration and invasion by downregulating vimentin expression and is a potential prognostic marker in breast cancer. Breast Cancer Res Treat. Aug; 2012 134(3):1081–1093. [PubMed: 22476851]
21. Liu X, Wang C, Chen Z, et al. MicroRNA-138 suppresses epithelial-mesenchymal transition in squamous cell carcinoma cell lines. Biochem J. Nov 15; 2011 440(1):23–31. [PubMed: 21770894]
22. Luo WR, Li SY, Cai LM, Yao KT. High expression of nuclear Snail, but not cytoplasmic staining, predicts poor survival in nasopharyngeal carcinoma. Ann Surg Oncol. Sep; 2012 19(9):2971–2979. [PubMed: 22476819]
23. Zhou BP, Deng J, Xia W, et al. Dual regulation of Snail by GSK-3beta-mediated phosphorylation in control of epithelial-mesenchymal transition. Nat Cell Biol. Oct; 2004 6(10):931–940. [PubMed: 15448698]
24. Du J, Sun B, Zhao X, et al. Hypoxia promotes vasculogenic mimicry formation by inducing epithelial-mesenchymal transition in ovarian carcinoma. Gynecol Oncol. Jun; 2014 133(3):575–583. [PubMed: 24589413]
25. Liu G, Sun Y, Ji P, et al. MiR-506 suppresses proliferation and induces senescence by directly targeting the CDK4/6-FOXM1 axis in ovarian cancer. J Pathol. Mar 6.2014
26. Hao L, Ha JR, Kuzel P, Garcia E, Persad S. Cadherin switch from E- to N-cadherin in melanoma progression is regulated by the PI3K/PTEN pathway through Twist and Snail. Br J Dermatol. Jun; 2012 166(6):1184–1197. [PubMed: 22332917]
27. Balli D, Ustiyan V, Zhang Y, et al. Foxm1 transcription factor is required for lung fibrosis and epithelial-to-mesenchymal transition. EMBO J. Jan 23; 2013 32(2):231–244. [PubMed: 23288041]
28. Yin M, Ren X, Zhang X, et al. Selective killing of lung cancer cells by miRNA-506 molecule through inhibiting NF-kappaB p65 to evoke reactive oxygen species generation and p53 activation. Oncogene. Jan 27.2014
29. Kuphal S, Bosserhoff AK. Influence of the cytoplasmic domain of E-cadherin on endogenous N-cadherin expression in malignant melanoma. Oncogene. Jan 12; 2006 25(2):248–259. [PubMed: 16132038]
30. Min C, Eddy SF, Sherr DH, Sonenshein GE. NF-kappaB and epithelial to mesenchymal transition of cancer. J Cell Biochem. Jun 1; 2008 104(3):733–744. [PubMed: 18253935]
31. Rodriguez MI, Peralta-Leal A, O'Valle F, et al. PARP-1 regulates metastatic melanoma through modulation of vimentin-induced malignant transformation. PLoS Genet. Jun.2013 9(6):e1003531. [PubMed: 23785295]
32. Hazan RB, Phillips GR, Qiao RF, Norton L, Aaronson SA. Exogenous expression of N-cadherin in breast cancer cells induces cell migration, invasion, and metastasis. J Cell Biol. Feb 21; 2000 148(4):779–790. [PubMed: 10684258]
33. Arora H, Qureshi R, Park WY. miR-506 regulates epithelial mesenchymal transition in breast cancer cell lines. PLoS One. 2013; 8(5):e64273. [PubMed: 23717581]
34. Wen SY, Lin Y, Yu YQ, et al. miR-506 acts as a tumor suppressor by directly targeting the hedgehog pathway transcription factor Gli3 in human cervical cancer. Oncogene. Mar 10.2014
35. Zhao Z, Ma X, Hsiao TH, et al. A high-content morphological screen identifies novel microRNAs that regulate neuroblastoma cell differentiation. Oncotarget. Feb 28.2014

36. Tivnan A, Orr WS, Gubala V, et al. Inhibition of neuroblastoma tumor growth by targeted delivery of microRNA-34a using anti-disialoganglioside GD2 coated nanoparticles. PLoS One. 2012; 7(5):e38129. [PubMed: 22662276]

37. Cubillos-Ruiz JR, Sempere LF, Conejo-Garcia JR. Good things come in small packages: Therapeutic anti-tumor immunity induced by microRNA nanoparticles. Oncoimmunology. Sep 1; 2012 1(6):968–970. [PubMed: 23162774]

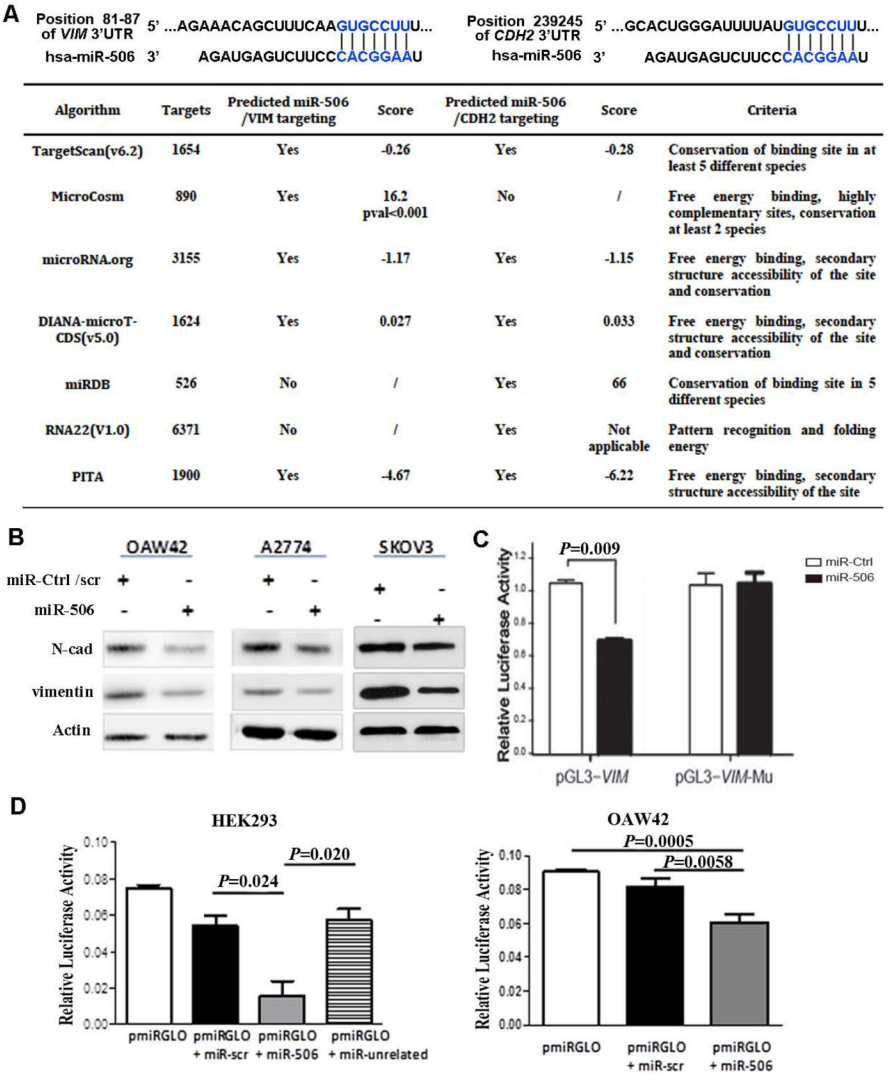

Algorithm	Targets	Predicted miR-506 /VIM targeting	Score	Predicted miR-506 /CDH2 targeting	Score	Criteria
TargetScan(v6.2)	1654	Yes	-0.26	Yes	-0.28	Conservation of binding site in at least 5 different species
MicroCosm	890	Yes	16.2 pval<0.001	No	/	Free energy binding, highly complementary sites, conservation at least 2 species
microRNA.org	3155	Yes	-1.17	Yes	-1.15	Free energy binding, secondary structure accessibility of the site and conservation
DIANA-microT-CDS(v5.0)	1624	Yes	0.027	Yes	0.033	Free energy binding, secondary structure accessibility of the site and conservation
miRDB	526	No	/	Yes	66	Conservation of binding site in 5 different species
RNA22(V1.0)	6371	No	/	Yes	Not applicable	Pattern recognition and folding energy
PITA	1900	Yes	-4.67	Yes	-6.22	Free energy binding, secondary structure accessibility of the site

Figure 1. MiR-506 directly targets *VIM* and *CDH2*

A. Prediction of miR-506 targeting *VIM*-3′UTR and *CDH2*-3′UTR. The predicted binding sites in *VIM*-3′UTR and *CDH2*-3′UTR are indicated by TargetScan software (top panel). The table summarizes the number of miR-506's targets, the criteria, and the prediction score for the 2 selected target genes in 7 algorithms. **B.** MiR-506 downregulated vimentin and N-cad protein expression in 3 EOC cell lines. Cells were transfected with hsa-miR-506 or miR-Ctrl/scrambled (scr) miR. Protein was collected at 48–96 hours post-transfection, and the expression of vimentin and N-cad was assessed by Western blot analysis. Actin was used as a control for protein loading. **C.** Luciferase assay indicates that miR-506 directly targets *VIM* through binding *VIM*-3′UTR. The full length of *VIM*-3′UTR was cloned into the pGL3 vector. The pGL3-*VIM*-mu vector has the sequence with the miR506 binding site deleted. SKOV3 cells were transfected with pGL3-Vim or pGL3-Vim-mu, together with miR-506 mimic or negative control miR. The relative luciferase activities were detected in 3 independent experiments. Error bars represent ± SD. **D.** Luciferase assay indicates that

miR-506 directly targets *CDH2* through binding *CDH2*-3′UTR in HEK293T and OAW42 OvCa cells. A small region of 25 bp of the *CDH2*-3′UTR containing the predicted miR-506 seed region was cloned into the pmiRGLO vector. HEK293T and OAW42 cells were transfected with pmiRGLO vector alone or in association with miR-506, a scrambled miR, or an unrelated miR. The relative luciferase activities were detected in 3 independent experiments. Error bars represent ± SD.

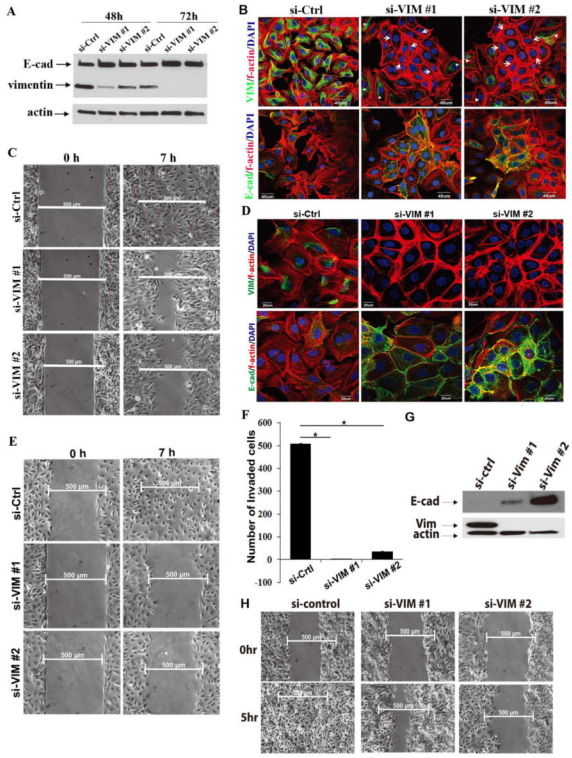

Figure 2. Attenuation of vimentin induces epithelial characteristics and suppresses cell migration and invasion in EOC cells

A. Attenuation of vimentin upregulates E-cad protein expression. OVCA433 cells were transfected with si-Ctrl, si-VIM #1, or si-VIM #2. Cell lysate was collected at 48 h and 72 h after siRNA transfection. The expression of vimentin and E-cad was detected using a Western blot analysis. Actin was used as a control. **B.** Attenuation of vimentin promotes epithelial cell morphological characteristics in mesenchymal EOC cells. OVCA433 cells were transfected with si-control, si-VIM #1, or si-VIM #2 for 72 hours. The cells were fixed and stained with vimentin or E-cad antibody. F-actin was stained by phalloidin-TRITC. Cell nuclei were stained with DAPI. Arrows indicate low vimentin-containing cells and epithelial f-actin morphological characteristics. Arrowheads indicate relatively high vimentin-containing cells and mesenchymal f-actin morphological characteristics. Scale bars represent 40 μm. **C.** Wound healing assay shows that vimentin knockdown inhibits the migration of EOC cells. OVCA433 cells from the same transfection as in **B** were seeded into a wound healing assay chamber. Images were taken at 0 h and 7 h after wound application. Scale bars represent 500 μm. **D.** The sustained knockdown of vimentin induces membrane E-cad expression, strengthens cell-cell adherence, and promotes epithelial morphological characteristics. OVCA433 cells were transfected with si-Ctrl, si-VIM #1, or si-VIM #2 3 times in a 4-day interval. At day 11 after transfection, OVCA433 cells were fixed and stained with vimentin/f-actin or E-cad/f-actin. Cell nuclei were stained with DAPI. Scale bars represent 20 μm. **E.** The sustained knockdown of vimentin dramatically inhibits cell migration. OVCA433 cells were from the same transfection as **D**. At day 11 after transfection, the cells were seeded into a wound healing assay chamber and images were taken at 0 h and 7 h after wound application. Scale bars represent 500 μm. **F.** The sustained

knockdown of vimentin significantly inhibits cell invasion. OVCA433 cells from the same transfection as in **D** were seeded into transwell invasion chambers (n=3) and allowed to invade for 20 hours. The cells that invaded the lower side of the transwell membrane were fixed and stained. The bar graph was generated by means ± SD from duplicate transwells for each group. *, P<0.001. **G.** Sustained knockdown of vimentin upregulates E-cad protein expression in SKOV3 cells. SKOV3 cells were transfected with si-Ctrl, si-VIM #1, or si-VIM #2 as in **D**. At day 11 post-transfection, cell lysate was collected and the expression of vimentin and E-cad was detected using a western blot analysis. Actin was used as a control. **H.** Sustained knockdown of vimentin inhibits SKOV3 migration. SKOV3 cells were transfected as in **G**. At day 11 post-transfection, SKOV3 cells were seeded into a wound healing assay chamber and cultured for 12 h. Images were taken at 0 h and 5 h after wound application. Scale bars represent 500μm.

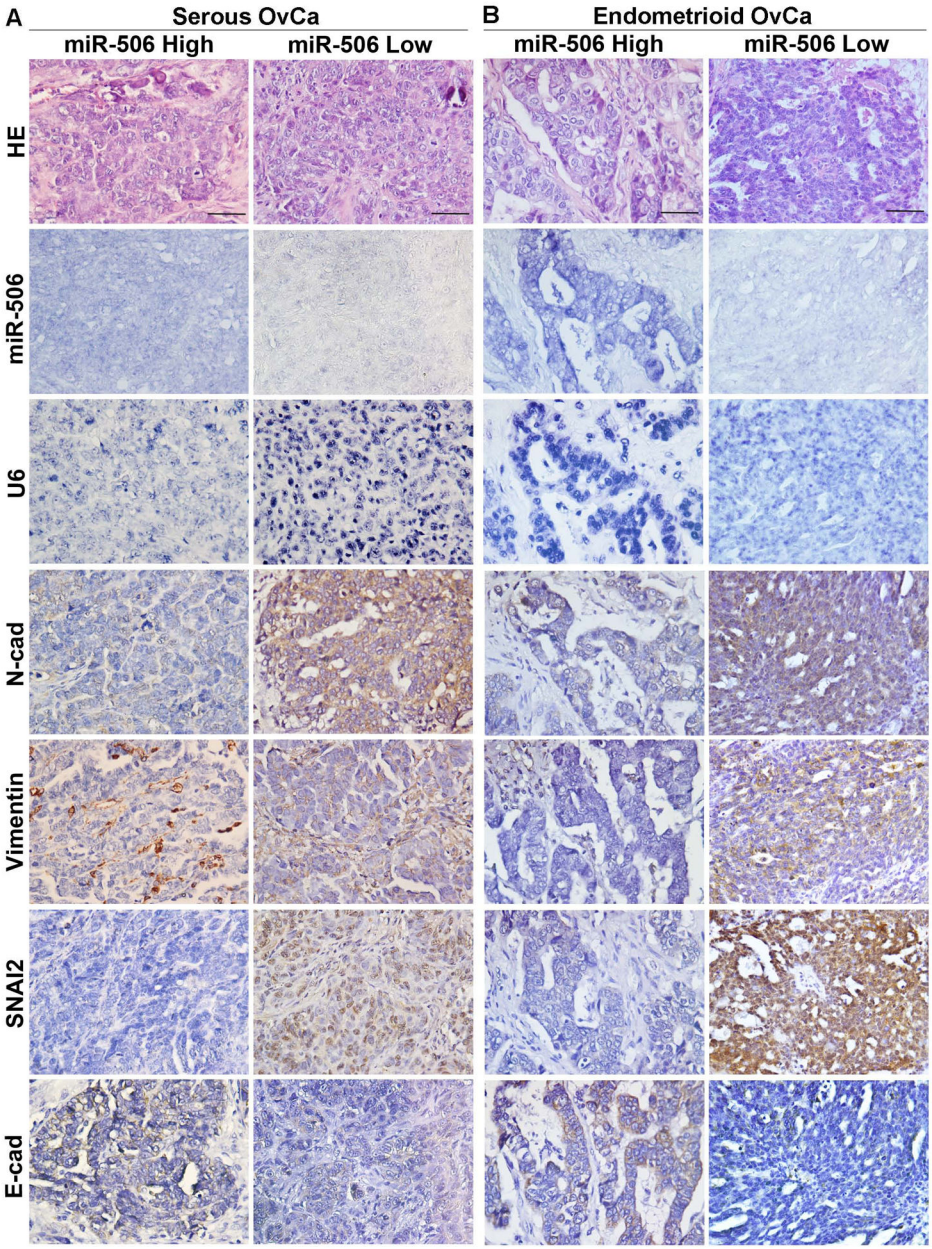

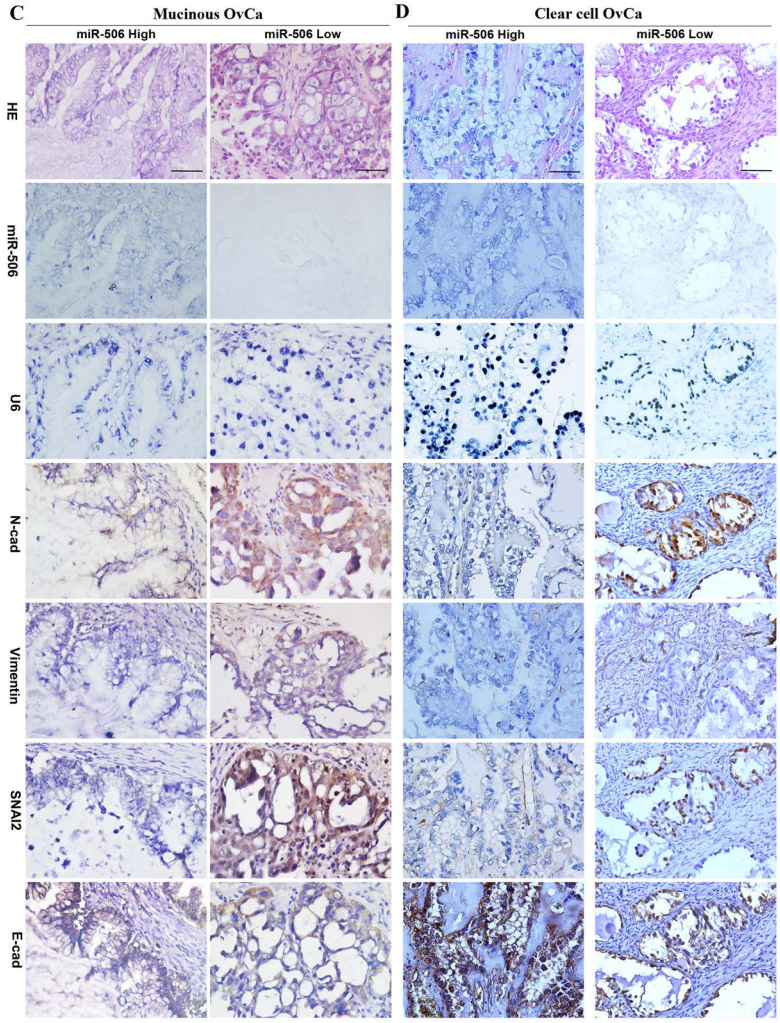

Figure 3. High miR-506 expression is associated with decreased N-cad, vimentin, and SNAI2 expression and increased E-cad expression in all major subtypes of EOC

MiR-506 ISH was performed using the double-DIG-labeled miRCURY LNA™ hsa-miR-506 probe (Exiqon) on TMA. The LNA U6 snRNA probe was used as a positive control for every case. Immunohistochemical staining was performed for N-cad, vimentin, SNAI2, and E-cad on the same TMA. The results of the statistical analyses are shown in Table 2. Representative images of all markers were taken at 400× magnification and shown on the basis of high and low miR-506 expression in high-grade serous (**A**), endometrioid (**B**), mucinous (**C**), and clear cell (**D**) OvCa. Scale bars represent 50 μm.

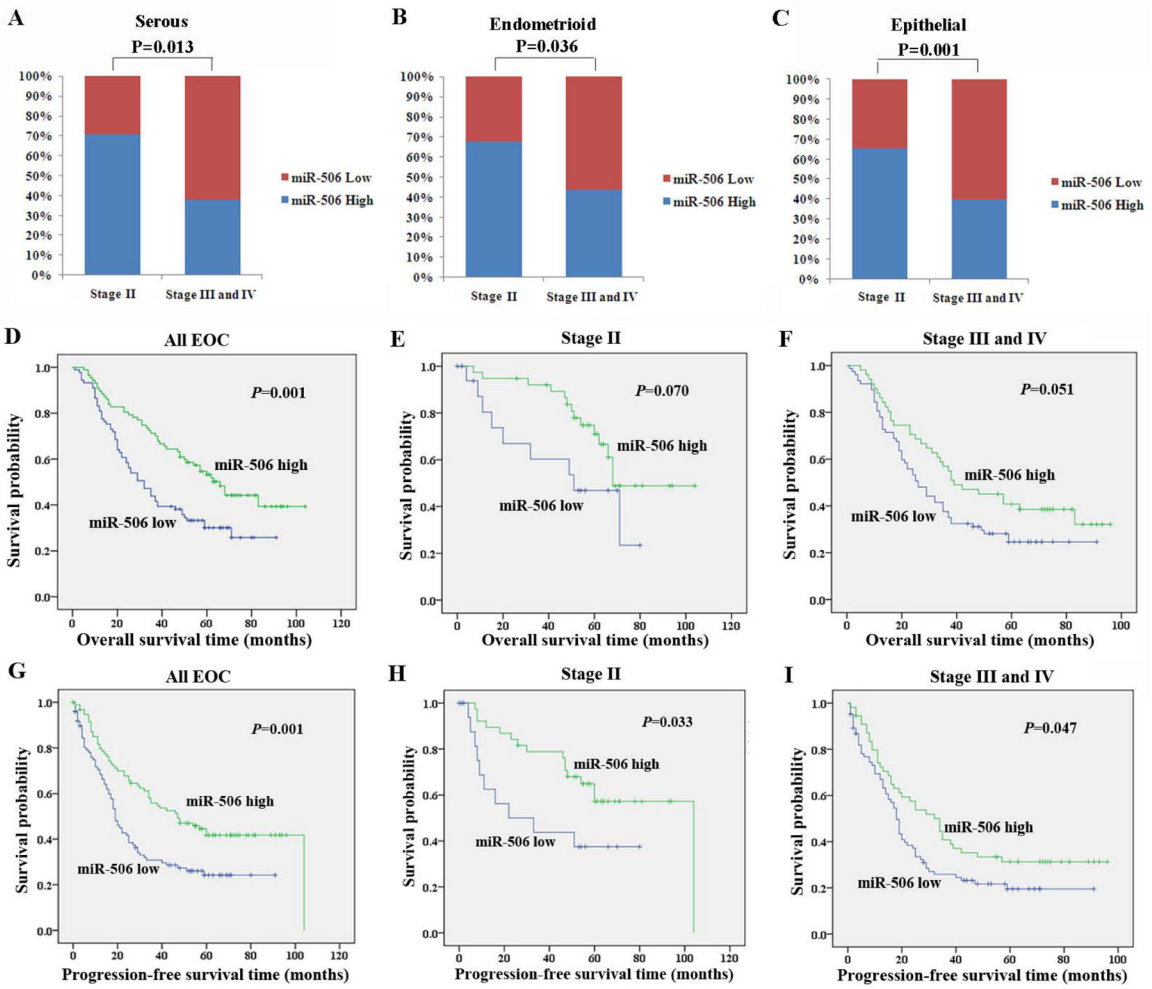

Figure 4. High miR-506 expression is associated with early FIGO stage and longer survival in patients with EOC

A–C. High miR-506 expression is associated with early FIGO stage in serous (**A**), endometrioid (**B**), and all EOC cases (C). MiR-506 was evaluated on TMAs by ISH and divided into high and low miR-506 expression according to the criteria described in the Methods. MiR-506 was analyzed in 99 serous, 74 endometrioid, and 197 EOC cases. **D–F.** High miR-506 expression is associated with longer overall survival (OS) in all EOC (**D**), stage II (**E**), and advanced-stage (stage III and IV) patients (**F**). **G–I**. High miR-506 expression is associated with longer progression-free survival (PFS) in all EOC (**D**), stage II (**E**), and advanced-stage (stage III and IV) patients (**F**).

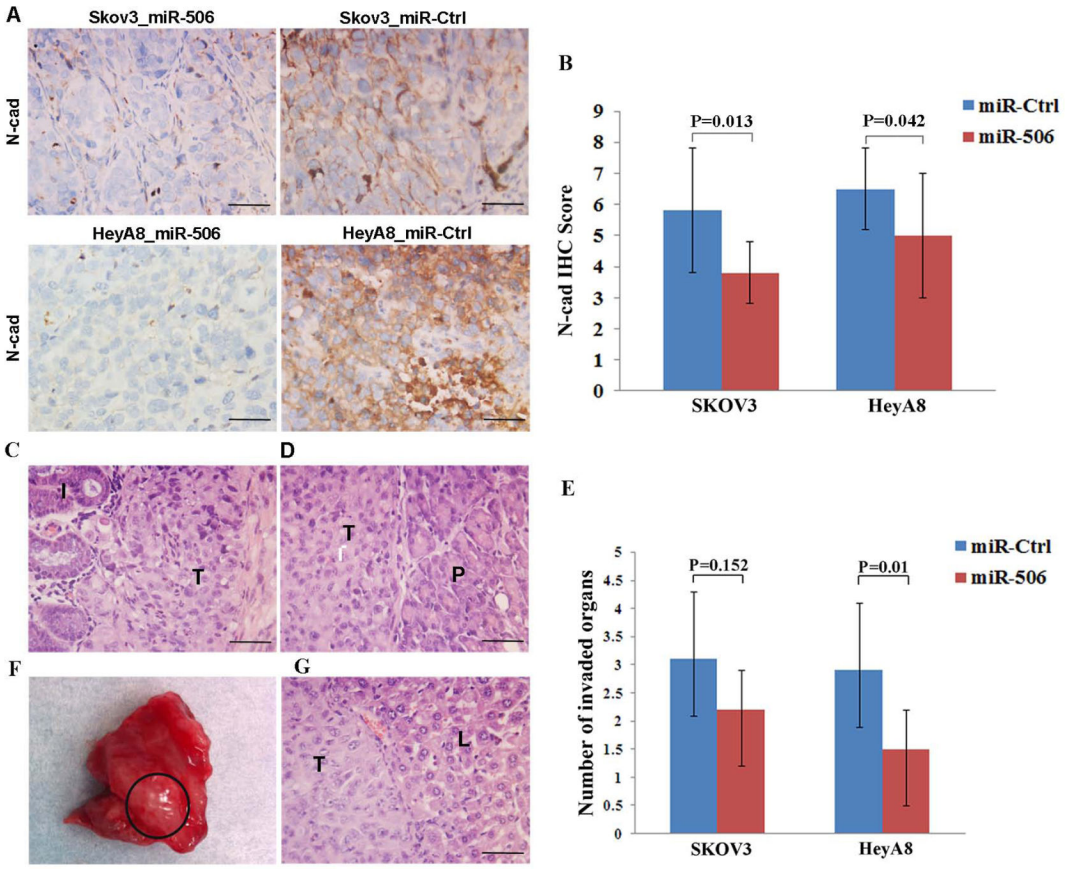

Figure 5. Systemic delivery of miR-506 suppresses invasion and metastasis of OvCa cells in mouse models

HeyA8-IP2 or SKOV3-IP1 cells were injected into the peritoneal cavities of nude mice. The mice were treated with miRNA incorporated in DOPC nanoliposomes (intraperitoneal administration): control miRNA/DOPC or miR-506/DOPC for each cell line (n = 10 mice per group), for 4–6 weeks. **A** and **B.** MiR-506 treatment led to decreased N-cad expression. Representative images of immunohistochemical staining for N-cad in 2 mouse models (**A**). The statistical analysis shows that N-cad expression is lower in the miR-506 treatment groups than in the miR-Ctrl treatment groups (**B**). **C.** SKOV3-IP3 cells invaded the intestines through the mesentery in the mice treated with miR-Ctrl. I, intestine; T, tumor cells. **D.** HeyA8-IP2 cells invaded the pancreases in the mice treated with miR-Ctrl. P, pancreas; T, tumor cells. **E.** The statistical analysis shows that the mean number of invaded organs by tumor cells in the miR-506 treatment groups is lower than in the miR-Ctrl treatment groups. **F** and **G.** Liver metastasis was found in 2 mice with HeyA8-IP2 cells and treated with miR-Ctrl. Shown is liver metastasis with no peri-hepatic or capsular invasion (**F**). H & E images of liver metastasis of HeyA8-IP2 cells (**G**). L, liver; T, tumor cells. Scale bars represent 50 μm.

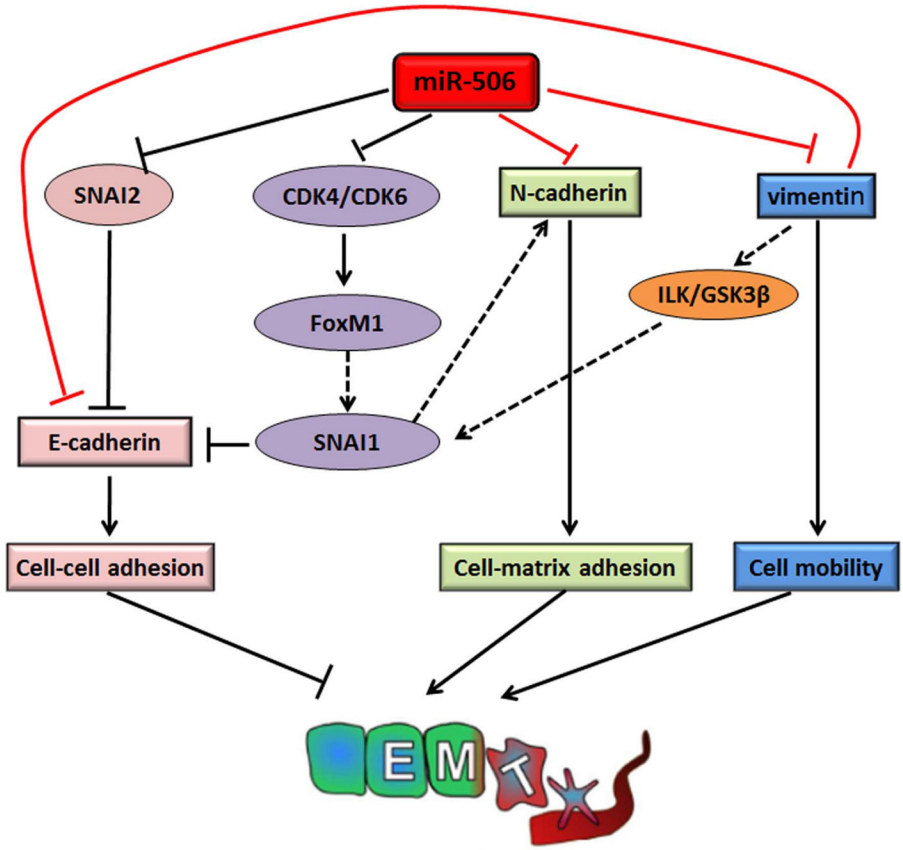

Figure 6. Summary of the role of miR-506 as a potent EMT inhibitor through targeting multiple EMT-related genes

MiR-506 directly targets SNAI2 [14], CDK4/CDK6 [25], vimentin, and N-cad. MiR-506 down-regulates SNAI2 and subsequently promotes cell-cell adherence via increasing E-cad expression. MiR-506 inhibits the expression of FoxM1 by directly down-regulating CDK4/CDK6, which decreases the activity of SNAI1 and eventually increases E-cad expression and decreases N-cad expression. Moreover, miR-506 directly down-regulates vimentin and N-cadherin, which reduces cell mobility and cell-matrix adherence. In addition, down-regulation of vimentin induces E-cadherin and increases cell-cell adherence. As a result, miR-506 suppresses EMT and cancer progression in EOC.

Table 1

Clinicopathological information on EOC patients in this study

Characteristic	Result
Number	204
Mean age, years (±SD)	55±10
Histology subtype, n (%)	
Serous	103 (50.5)
Endometrioid	76 (37.3)
Mucinous	10 (4.9)
Clear cell	8 (3.9)
Transitional cell	1 (0.5)
Mixed	4 (2.0)
Undifferentiated	2 (1.0)
Grade, n (%)	
G1	11 (5.3)
G2	68 (33.0)
G3	125 (60.7)
Stage, n (%)	
II	59 (28.9)
III	124 (60.8)
IV	20 (9.8)
No information	1(0.5)
Median follow-up, months (range)	38 (1–104)

Table 2

Expression of miR-506 and epithelial and mesenchymal proteins in EOC cases on TMA (mean±SD)*

Subtype	n	N-cadherin	Vimentin	Snai2	E-cadherin
Serous					
MiR-506 high	43	5.5±2.3	1.0±0.3	3.0±2.0	8.8±1.2
MiR-506 low	56	7.4±2.6	4.0±1.8	5.0±2.7	6.0±2.0
p-value		<0.001	<0.001	<0.001	<0.001
Endometrioid					
MiR-506 high	39	5.5±2.7	1.0±0.2	3.8±2.7	8.9±2.0
MiR-506 low	35	7.5±2.6	3.9±1.0	5.2±2.5	6.5±0.5
p-value		0.002	<0.001	0.025	<0.001
Mucinous					
MiR-506 high	3	3.5±2.0	1.2±0.7	2.5±1.7	8.5±1.2
MiR-506 low	6	7.0±3.5	4.3±2.0	7.0±1.7	4.5±1.5
p-value		0.087	0.087	0.008	0.003
Clear cell					
MiR-506 high	4	3.2±1.9	1.2±0.5	3.0±2.1	9.0±0
MiR-506 low	4	9.0±0	4.0±1.4	6.8±1.5	7.5±1.3
p-value		0.001	0.010	0.029	0.134
All EOC					
MiR-506 high	95	5.2±2.5	1.0±0.6	3.3±2.1	8.8±2.0
MiR-506 low	102	7.3±2.8	4.0±1.9	5.2±2.7	6.3±0.9
p-value		<0.001	<0.001	<0.001	<0.001

*Numbers are referred to mean±SD of scores as defined in Material and Methods.